J|A|C|S
ARTICLES
Published on Web 08/15/2002

Spectroscopic and Computational Studies on Iron and Manganese Superoxide Dismutases: Nature of the Chemical Events Associated with Active-Site pKs

Timothy A. Jackson,[†] Juan Xie,[†] Emine Yikilmaz,[‡] Anne-Frances Miller,[‡] and Thomas C. Brunold*,[†]

Contribution from the Department of Chemistry, University of Wisconsin—Madison, Madison Wisconsin 53706 and Department of Chemistry, University of Kentucky, Lexington, Kentucky 40506

Received April 19, 2002

Abstract: A combined spectroscopic/computational approach has been utilized to explore the chemical origins of the active-site p*K*s of the structurally homologous Fe- and Mn-dependent superoxide dismutases (SODs). Absorption, circular dichroism, magnetic circular dichroism, and variable-temperature, variable-field magnetic circular dichroism spectroscopic experiments have permitted us to determine electronic transition energies and polarizations, as well as ground-state spin Hamiltonian parameters. These experimental data have been used in conjunction with semiempirical intermediate neglect of differential overlap/spectroscopic parametrization configuration interaction (INDO/S-CI) computations for evaluating hypothetical active-site models for the high-pH species generated by density functional theory (DFT) geometry optimizations. Our experimental and computational data indicate that both reduced FeSOD and oxidized MnSOD do not bind hydroxide at high pH; rather, the active-site p*K* for these two species is attributed to deprotonation of a second-sphere tyrosine. Conversely, our data obtained on oxidized FeSOD indicate that hydroxide binding is responsible for the observed active-site p*K* for this species. Intriguingly, in the Fe-substituted form of MnSOD this identical chemical event occurs at a significantly lower pH. Overall, our results suggest an important role for second-sphere amino acids in tuning the active sites' interaction with small anions and bring into question the assumption that these homologous enzymes operate by the same molecular mechanism.

1. Introduction

Superoxide dismutases (SODs)[1] are metalloenzymes whose function is to disarm the superoxide radical anion ($O_2^{\cdot -}$).[2,3] As all aerobic species are susceptible to oxidative damage caused by superoxide, nature has evolved several forms of SODs that contain either Fe, Mn, Cu/Zn, or Ni active sites.[2,4] Fe- and Mn-dependent SODs function analogously by disproportionating superoxide in a two-step ping-pong mechanism in which the metal ion M (corresponding to Fe or Mn) cycles between the +3 and +2 oxidation states (eqs 1a,b),[5,6] which presumably bind coordinated solvent in the hydroxo and aqua forms, respectively (eq 2).[7,8]

$$M^{3+}SOD + O_2^{\cdot -} + 1H^+ \rightarrow M^{2+}SOD\text{-}H^+ + O_2 \quad (1a)$$

$$M^{2+}SOD\text{-}H^+ + O_2^{\cdot -} + 1H^+ \rightarrow M^{3+}SOD + H_2O_2 \quad (1b)$$

$$M^{3+}\text{-}OH + 1e^- + 1H^+ \rightarrow M^{2+}\text{-}OH_2 \quad (2)$$

Fe- and MnSODs are structurally homologous, possessing similar protein folds as well as virtually identical first- and second-sphere coordination shells (Figure 1).[9−11] In both

* To whom correspondence should be addressed: 1101 University Ave., Madison, WI 53706. Phone (608) 265-9056; fax (608) 262-6143; e-mail Brunold@chem.wisc.edu.

[†] University of Wisconsin—Madison.

[‡] University of Kentucky.

(1) Abbreviations: ADF, Amsterdam density functional; CAPS, 3-cyclohexylamino-1-propanesulfonic acid; CD, circular dichroism; CI, configuration interaction; CT, charge transfer; DFT, density functional theory; DOMO, doubly occupied molecular orbital; E_m, reduction midpoint potential; EPR, electron paramagnetic resonance; HOMO, highest occupied molecular orbital; INDO/S, intermediate neglect of differential overlap/spectroscopic parametrization; LF, ligand-field; LMCT, ligand-to-metal charge transfer; LUMO, lowest unoccupied molecular orbital; MCD, magnetic circular dichroism; MO, molecular orbital; NMR, nuclear magnetic resonance; PDB, protein data bank; SOD, superoxide dismutase; SOMO, singly occupied molecular orbital; VTVH, variable-temperature, variable-field; ZFS, zero-field splitting; ZPE, zero-point energy.

(2) Miller, A. F.; Sorkin, D. L. *Comments Mol. Cell. Biophys.* **1997**, *9*, 1−48.
(3) Valentine, J. S.; Wertz, D. L.; Lyons, T. J.; Liou, L.; Goto, J. J.; Gralla, E. B. *Curr. Opin. Chem. Biol.* **1998**, *2*, 253−262.
(4) Choudhury, S. B.; Lee, J. W.; Davidson, G.; Yim, Y. I.; Bose, K.; Sharma, M. L.; Kang, S. O.; Cabelli, D. E.; Maroney, M. J. *Biochemistry* **1999**, *38*, 3744−3752.
(5) Bull, C.; Fee, J. A. *J. Am. Chem. Soc.* **1985**, *107*, 3295−3304.
(6) Bull, C.; Niederhoffer, E. C.; Yoshida, T.; Fee, J. A. *J. Am. Chem. Soc.* **1991**, *113*, 4069−4076.
(7) Tierney, D. L.; Fee, J. A.; Ludwig, M. L.; Penner-Hahn, J. E. *Biochemistry* **1995**, *34*, 1661−1668.
(8) Stallings, W. C.; Metzger, A. L.; Pattridge, K. A.; Fee, J. A.; Ludwig, M. L. *Free Radical Res. Commun.* **1991**, *12−13*, 259−268.
(9) Lah, M. S.; Dixon, M. M.; Pattridge, K. A.; Stallings, W. C.; Fee, J. A.; Ludwig, M. L. *Biochemistry* **1995**, *34*, 1646−1660.
(10) Edwards, R. A.; Baker, H. M.; Whittaker, M. M.; Whittaker, J. W.; Jameson, G. B.; Baker, E. N. *J. Biol. Inorg. Chem.* **1998**, *3*, 161−171.
(11) Ludwig, M. L.; Metzger, A. L.; Pattridge, K. A.; Stallings, W. C. *J. Mol. Biol.* **1991**, *219*, 335−358.

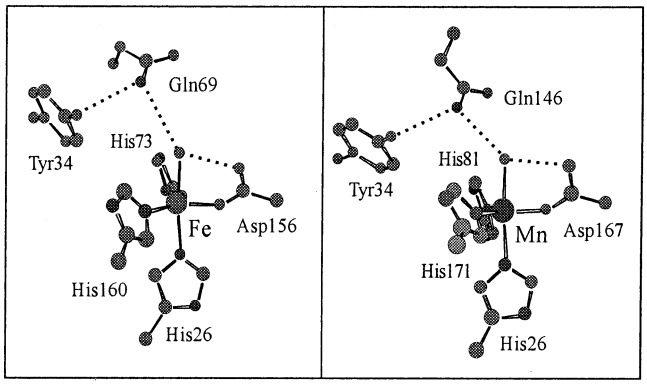

Figure 1. Active-site models of Fe^{3+}SOD (left) and Mn^{3+}SOD (right), based on coordinates from the protein data bank files 1ISB and 3MDS, respectively.

enzymes the metal ion is bound in a trigonal bipyramidal geometry with two histidines and an aspartate residue in the equatorial plane and a third histidine residue and a coordinated solvent as axial ligands (Figure 1). This coordinated solvent is involved in a hydrogen-bonding network with a glutamine residue (Q69 for FeSOD[9] and Q146 for MnSOD[10] from *Escherichia coli*) that in turn hydrogen-bonds with a universally conserved tyrosine (Y34) residue.

Despite the extraordinary similarity of these enzymes, the *E. coli* Fe- and MnSODs exhibit metal ion specificity with respect to enzymatic activity; i.e., Fe incorporated into the MnSOD protein matrix [Fe(Mn)SOD] is catalytically inactive, as is Mn(Fe)SOD.[12,13] Various factors have been proposed to contribute to the lack of activity of the metal-substituted enzymes; e.g., differences in redox tuning and active-site p*K* values imparted by the subtly different protein matrixes.[13b−18] However, a detailed understanding of the mechanism by which these differences arise has yet to be developed. While redox tuning of the transition metal ions could in principle occur through changes in the geometric and electronic environment created by the ligand field, the Fe- and MnSOD active sites are virtually identical (Figure 1). Therefore, it has been proposed that the hydrogen-bond network involving the coordinated solvent exerts a large influence on redox tuning.[16,19] This is consistent with the observations that Fe(Mn)SOD displays an active-site p*K*, associated with different EPR consequences, 2 pH units below that of FeSOD and that Fe(Mn)SOD gains significant catalytic activity at low pH [for Fe(Mn)SOD at pH 7.8, activity is 60 units/mg, while for Fe(Mn)SOD at pH 6.3, activity increases to 480 units/mg, roughly 8% of the activity of FeSOD[14]]. Indeed, pH-dependent events are expected to play a major role in tuning active-site properties since protonation of active-site residues will tend to restore Fe(Mn)SOD's very low E_m.[14,16]

Besides their relevance to metal ion specificity, active-site p*K*s of Fe- and MnSOD also have important mechanistic implications, as two protons are required for turnover (eq 1).[5] One possible proton donor is the coordinated solvent molecule (Figure 1), as it is proposed to shuttle between the hydroxo and aqua forms depending on the oxidation state of the metal (eq 2).[7,8] A titratable active-site residue, for which tyrosine 34 seems a likely candidate, may provide the second proton necessary for catalysis.

Due to the importance of pH effects in Fe- and MnSODs, much effort has gone into accurately determining p*K* values. By use of optical spectroscopy, it has been shown that the oxidized proteins, Fe^{3+}SOD and Mn^{3+}SOD, have active-site p*K*s of 8.5−9 and 9.6−10 pH units, respectively.[5,14,20] As the Fe^{3+}-SOD active-site p*K* is associated with a reduction in activity due to an increase in K_m, it has been interpreted in terms of binding of a hydroxide ion to the five-coordinate active site.[7] Additional support for this proposal is provided by crystallographic studies of a cambialistic (i.e., not metal ion specific) FeSOD from *Propionibacterium shermanii*, which revealed that the coordination number at the ferric site changes from 5 to 6 as pH is increased.[21] In the case of Mn^{3+}SOD, however, the chemical nature of the p*K* is less clear. A recent crystallographic study of *E. coli* MnSOD crystals grown at pH 8.5 and cryocooled to 100 K revealed partial occupancy (20−43%) of the open coordination site of the Mn ion by a solvent molecule.[22] However, the MnSOD protein in this study was a mixture of the +2 and +3 oxidation states. Thus, it cannot be determined if solvent binds to the Mn^{2+}, Mn^{3+}, or both sites at high pH or whether the solvent molecule identified crystallographically is hydroxide or water. Finally, site-directed mutagenesis of second-sphere amino acids such as Y34 (Figure 1) to phenylalanine appreciably reduces the optical changes observed for Mn^{3+}SOD upon increasing pH,[14,23] leaving the identity of the high-pH species of wild-type Mn^{3+}SOD unclear.

Spectroscopic studies of the reduced forms of the enzymes, Fe^{2+}SOD and Mn^{2+}SOD, have also permitted identification of active-site p*K*s. For Fe^{2+}SOD, NMR spectroscopy has been used to show that the active site has a p*K* of 8.5 that is eliminated when Y34 is mutated to phenylalanine.[24] EPR spectroscopy indicates that Mn^{2+}SOD undergoes major spectroscopic changes at high pH occurring at a p$K \sim 10.5$.[25]

Thus, despite much research, the exact natures of the p*K* transitions of FeSOD and MnSOD (e.g., the identities of the high-pH species) are still unclear. We have used electronic absorption, circular dichrosim (CD), and magnetic circular dichroism (MCD) spectroscopies to compare the electronic transition energies and ground-state spin Hamiltonian parameters of neutral and high-pH forms of oxidized and reduced FeSOD as well as oxidized MnSOD. These experimental data are used in conjunction with semiempirical INDO/S-CI computations to evaluate hypothetical active-site models generated by density functional theory (DFT) energy minimizations. Our data suggest that at high pH a competition exists between hydroxide binding

(12) Ose, D. E.; Fridovich, I. *J. Biol. Chem.* **1976**, *251*, 1217−1218.
(13) (a) Yamakura, F. *J. Biochem. (Tokyo)* **1978**, *83*, 849−857. (b) Yamakura, F.; Kobayashi, K.; Ue, H.; Konno, M. *Eur. J. Biochem.* **1995**, *227*, 700−706.
(14) Whittaker, M. M.; Whittaker, J. W. *Biochemistry* **1997**, *36*, 8923−8931.
(15) Edwards, R. A.; Whittaker, M. M.; Whittaker, J. W.; Jameson, G. B.; Baker, E. N. *J. Am. Chem. Soc.* **1998**, *120*, 9684−9685.
(16) Vance, C. K.; Miller, A.-F. *J. Am. Chem. Soc.* **1998**, *120*, 461−467.
(17) Vance, C. K.; Miller, A.-F. *Biochemistry* **1998**, *37*, 5518−5527.
(18) Vance, C. K.; Miller, A. F. *Biochemistry* **2001**, *40*, 13079−13087.
(19) Yikilmaz, E.; Xie, J.; Brunold, T. C.; Miller, A. F. *J. Am. Chem. Soc.* **2002**, *124*, 3482−3483.
(20) Fee, J. A.; McClune, G. J.; Lees, A. C.; Zidovetzki, R.; Pecht, I. *Isr. J. Chem* **1981**, *21*, 54−58.
(21) Schmidt, M. *Eur. J. Biochem.* **1999**, *262*, 117−126.
(22) Børgstahl, G. E. O.; Pokross, M.; Chehab, R.; Sekher, A.; Snell, E. H. *J. Mol. Biol.* **2000**, *296*, 951−959.
(23) Edwards, R. A.; Whittaker, M.; Whittaker, J.; Baker, E. N.; Jameson, G. B. *Biochemistry* **2001**, *40*, 4622−4632.
(24) Sorkin, D. L.; Duong, D. K.; Miller, A.-F. *Biochemistry* **1997**, *36*, 8202−8208.
(25) Maliekal, C. Vance, A. Karapetian, and A. F. Miller, unpublished results.

to the active-site metal and deprotonation of tyrosine 34. Possible mechanistic implications of our results are discussed.

2. Experimental Section

Protein Species. Wild-type FeSOD and MnSOD were purified from *E. coli* according to published procedures.[26,27] The specific activities of purified FeSOD and MnSOD were >6000 units (mg of protein)$^{-1}$ min^{-1}, respectively. Fe(Mn)SOD was prepared according to published procedures[17] in which MnSOD was treated with guanidine hydrochloride and EDTA to generate partially unfolded apo-MnSOD that was subsequently reconstituted with Fe. Both Fe- and MnSODs were isolated predominantly in the oxidized state. Reduced FeSOD was generated by the following procedure. A solution of ~1 mM Fe^{3+}SOD was sealed in a vial that was purged with argon for ~30 min. To this solution was added a 2-fold molar excess of freshly prepared dithionite in 100 mM potassium hydroxide.

Spectroscopy. Variable-temperature absorption, CD, and MCD spectra were recorded on a Jasco J-715 spectropolarimeter in conjunction with an Oxford Instruments SM-4000 8T magnetocryostat. All low-temperature CD and MCD data were taken in 55% (v/v) glycerol and appropriate buffer. All neutral samples were prepared in 50 mM potassium phosphate buffer, pH 7.0. High-pH samples of Fe^{2+}SOD and Mn^{3+}SOD were prepared in 100 mM 3-cyclohexylamino-1-propanesulfonic acid (CAPS) buffer, pH 11.0, while high-pH samples of Fe^{3+}SOD and Fe^{3+}(Mn)SOD were prepared in pH 10 CAPS buffer. The N_3-Mn^{3+}SOD adduct was prepared by generating a solution 0.946 mM in Mn^{3+} sites and 188 mM in azide (since K_d = 2.2 mM,[5] this azide/protein ratio ensures complete conversion of Mn^{3+}SOD to N_3-Mn^{3+}SOD). VTVH MCD data were analyzed with a fitting program developed by Dr. Frank Neese.[28]

Computations. A. Active-Site Geometry. Active-site models for various forms of Fe- and MnSODs were taken from their respective PDB files. In all cases, the Asp and His ligands were replaced by formate and amines, respectively, while the second-sphere Tyr and Gln residues were modeled by 4-methylphenol and acetamide, respectively. In some instances additional modifications were made, as described in the Results and Analysis section. The Cartesian coordinates of all active-site models used in this study are included as Supporting Information (Tables S1−S11).

B. DFT Calculations. DFT energy minimizations were performed with the Amsterdam Density Functional (ADF) 2000.02 software package.[29−32] These computations were carried out on a home-built cluster of eight Pentium III processors using ADF basis set II, an integration constant of 4.0, and the Vosko−Wilk−Nusair[33] local density approximation with the nonlocal gradient corrections of Becke[34] and Perdew.[35] Core orbitals were frozen through 1s (O, N, C), and 3p (Fe, Mn). For all species, the coordinates of the solvent ligand, the hydrogen atoms involved in the conserved hydrogen-bond network (Figure 1, dotted line), and exogenous ligands (i.e., azide or an equatorially bound hydroxide) were DFT energy-minimized, while all other coordinates were kept fixed.

Single-point DFT calculations were performed on these optimized structures with the ORCA 2.0 software package developed by Dr. Frank Neese (MPI Mülheim, Germany).[28] For all ORCA calculations, a Gaussian polarized double-ζ valence orbital basis set and the Demon_J auxiliary basis set were used with the Becke X−Perdew 86 correlation functional.[36] The size of the integration grid used was 3 (Lebedew 194 points). While the results obtained from DFT calculations with the ADF 2000.02 and ORCA 2.0 software packages were virtually identical, the latter has the great advantage that boundary surface plots of molecular orbitals can be generated with the gOpenMol program developed by Laaksonen.[37,38]

C. Semiempirical Calculations. The ORCA 2.0 software package was also used to perform semiempirical INDO/S-CI calculations on geometry-optimized active-site models. The ORCA program uses the INDO/S-CI model of Zerner and co-workers,[39,40] the valence shell ionization potentials and Slater−Condon parameters listed by Bacon and Zerner,[41] the standard interaction factors $f_{p\sigma p\sigma} = 1.266$ and $f_{p\pi p\pi} = 0.585$, and the following spin−orbit coupling constants: $\zeta_{3d}(Fe) = 400$ cm^{-1}, $\zeta_{4p}(Fe) = 445$ cm^{-1}, $\zeta_{3d}(N) = 300$ cm^{-1}, $\zeta_{4p}(Mn) = 334$ cm^{-1}, $\zeta_{2p}(N) = 76$ cm^{-1}, and $\zeta_{2p}(O) = 150$ cm^{-1}. Restricted open-shell Hartree−Fock (ROHF) SCF calculations were tightly converged on the sextet (for Fe^{3+}- and Mn^{2+}-containing active-site models) or quintet (for the Fe^{2+}- and Mn^{3+}SOD models) ground state that served as the reference state for configuration interaction (CI) calculations. Electronic transition energies were calculated by including single-electron excitations from all doubly occupied MOs (DOMOs) within 5 eV of the HOMO to the five (Fe^{3+} and Mn^{2+}SOD models) or four (Fe^{2+} and Mn^{3+}SOD models) singly occupied MOs (SOMOs) and to all virtual MOs within 5 eV of the LUMO, as well as including spin-allowed excitations from all SOMOs to all virtual MOs within 5 eV of the LUMO. Calculations to determine electronic transition energies also included spin-forbidden excitations [i.e., sextet to quartet transitions (Fe^{3+} and Mn^{2+}) and quintet to triplet transitions (Fe^{2+} and Mn^{3+})] within the Fe 3d- or Mn 3d-based SOMOs and the Mn 3d-based virtual MO (in the case of Mn^{3+}SOD). Larger active spaces did not significantly change calculated electronic transition energies and intensities. Ground-state calculations also included double-electron excitations from DOMOs within 2 eV of the HOMO to all SOMOs and to virtual MOs within 2 eV of the LUMO. The specific number of single- and double-electron excitations included for each active-site model discussed in the text is available as Supporting Information. For additional details on INDO/S-CI calculations using the ORCA software package, see ref 28 and literature cited therein.

D. ΔpK Calculations. Following a scheme developed by Noodleman and co-workers,[42−44] the pK value associated with proton transfer can be calculated as follows:

$$pK[M^{x+}\text{-SOD}] = \{PA_{(g)} + \Delta\epsilon_{sol-PT} - 267.7\}/1.37 \qquad (3)$$

$$PA_{(g)} = \epsilon_{deprot} + \Delta ZPE + {}^5/_2 RT \qquad (4)$$

where $PA_{(g)}$ is the system's gas-phase proton affinity in kilocalories per mole, $\Delta\epsilon_{sol-PT}$ is the difference in solvation energies of the deprotonated and protonated states, −267.7 kcal/mol is a correction term associated with the proton free energy in aqueous medium, ϵ_{deprot} is the gas-phase deprotonation energy, and ΔZPE is the zero-point energy difference between the deprotonated and protonated states. In this study we have determined ϵ_{deprot} by taking the difference between predicted DFT energies of the deprotonated and protonated forms of Fe- and MnSODs:

(26) Slykhouse, T. O.; Fee, J. A. *J. Biol. Chem.* **1976**, *251*, 5472−5477.
(27) Sorkin, D. L.; Miller, A.-F. *Biochemistry* **1997**, *36*, 4916−4924.
(28) Neese, F.; Solomon, E. I. *Inorg. Chem.* **1999**, *38*, 1847−1865.
(29) Baerends, E. J.; Ellis, D. E.; Ros, P. *Chem. Phys.* **1973**, *2*, 41.
(30) Versluis, L.; Ziegler, T. *J. Chem. Phys.* **1988**, *88*, 322−328.
(31) te Velde, G.; Baerends, E. J. *J. Comput. Phys.* **1992**, *99*, 84−98.
(32) Guerra, C. F.; Snijders, J. G.; te Velde, G.; Baerends, E. J. *Theor. Chem. Acc.* **1998**, *99*, 391−403.
(33) Vosko, S. H.; Wilk, L.; Nusair, M. *Can. J. Phys.* **1980**, *58*, 1200.
(34) Becke, A. D. *J. Chem. Phys.* **1986**, *84*, 4524−4529.
(35) Perdew, J. P. *Phys. Rev. B* **1986**, *33*, 8822−8824.
(36) Godbout, N.; Salahub, J.; Andzelm, J.; Wimmer, E. *Can. J. Chem.* **1992**, *70*, 560.
(37) Laaksonen, L. *J. Mol. Graphics* **1992**, *10*, 33.
(38) Bergman, D. L.; Laaksonen, L.; Laaksonen, A. *J. Mol. Graphics Modell.* **1997**, *15*, 301.
(39) Ridley, J.; Zerner, M. C. *Theor. Chim. Acta* **1973**, *32*, 111.
(40) Zerner, M. C.; Loew, G. H.; Kirchner, R. F.; Mueller-Westerhof, U. T. *J. Am. Chem. Soc.* **1980**, *102*, 589.
(41) Bacon, A. D.; Zerner, M. C. *Theor. Chim. Acta* **1979**, *53*, 21.
(42) Li, J.; Fisher, C. L.; Chen, J. L.; Bashford, D.; Noodleman, L. *Inorg. Chem.* **1996**, *35*, 4694−4702.
(43) Konecny, R.; Li, J.; Fisher, C. L.; Dillet, V.; Bashford, D.; Noodleman, L. *Inorg. Chem.* **1999**, *38*, 940−950.
(44) Han, W.-G.; Lovell, T.; Noodleman, L. *Inorg. Chem.* **2002**, *41*, 205−218.

$$\epsilon_{\text{deprot}} = \epsilon[M^{x+}\text{-SOD}^{OH}] + \epsilon[H^+] - \epsilon[M^{x+}\text{-SOD}^{H_2O}] \quad (5)$$

As can be seen from eqs 3 and 4, the calculation of absolute p*K* values requires the accurate prediction of differences in solvation and zero-point energies between deprotonated and protonated states, which is computationally rather difficult.[43] In calculating a ΔpK, we can ignore these contributions under the assumption that changes in solvation energies and zero-point energies are similar within the SOD family. Importantly, the active-site models that we compare for our Δp*K* calculations retain overall active-site charge with respect to one another. Thus, eqs 3 and 4 reduce to eqs 6 and 7, respectively. This ΔpK can then be used as a means to compare active-site p*K*s associated with solvent deprotonation or hydroxide binding.

$$\Delta pK = \{\Delta PA_{(g)}\}/1.37 \quad (6)$$

$$\Delta PA_{(g)} = \epsilon_{\text{deprot}}[Mn^{x+}\text{-SOD}] - \epsilon_{\text{deprot}}[Fe^{x+}\text{-SOD}] \quad (7)$$

3. Results and Analysis

3.1 General Approach. Spectroscopy. Absorption, CD, and MCD spectroscopies have been used to gain geometric and electronic structure information on the active sites of Fe- and MnSODs at neutral and high pH. While all of these techniques probe electronic transitions, the different selection rules involved in these spectroscopies allow for a more complete understanding of electronic properties.[45] Absorption selection rules dictate that a transition must be both electric dipole- and spin-allowed. Consequently, d → d (ligand field, LF) transitions are typically weak in an absorption spectrum, while ligand-to-metal charge transfer (LMCT) transitions usually carry significant intensity. CD spectroscopic selection rules require that a transition be both electric and magnetic dipole-allowed; thus, more insight can be gained into the origin of an electronic transition through the complementary use of absorption and CD spectroscopies. MCD selection rules require a transition to have two perpendicular transition moments. For metalloprotein active sites that inherently possess low symmetry, this selection rule requires spin−orbit coupling between excited states. As this coupling is most effective among ligand field excited states, d → d transitions are typically more intense relative to CT transitions in an MCD spectrum than in an absorption spectrum. Spin−orbit coupling can also occur between LF excited states and LMCT excited states, allowing spin-forbidden d → d transitions to gain intensity. Additionally, MCD intensity saturation behavior can give insight into ground-state spin Hamiltonian parameters [e.g., *g* values, as well as axial and rhombic zero-field splitting (ZFS) parameters *D* and *E*, respectively] and electronic transition polarizations.[28,46] Together, these three spectroscopic techniques permit the determination of electronic transition energies and polarizations along with ground-state spin Hamiltonian parameters.

Computations. Our computational approach involved three steps. (i) X-ray crystal structure coordinates were used as a starting point for DFT geometry optimizations in order to energy-minimize hydrogen-bond networks or, in the case of structurally ill-defined species (e.g., Fe^{3+}SOD at high pH), to optimize the coordinates of putative exogenous ligands (e.g., hydroxide ion) through energy minimization. (ii) Semiempirical INDO/S-CI computations were performed on these DFT energy-minimized hypothetical active sites in order to predict corresponding spectroscopic parameters that were compared with our experimental data. When a high level of agreement was achieved between calculated and experimental data, the model was assumed to be a reasonable description of the species studied, whereas poor agreement indicated that the hypothetical model used needed to be altered until better agreement was achieved. (iii) Single-point DFT computations were performed on the experimentally validated active-site models to generate quantitative electronic structure descriptions.

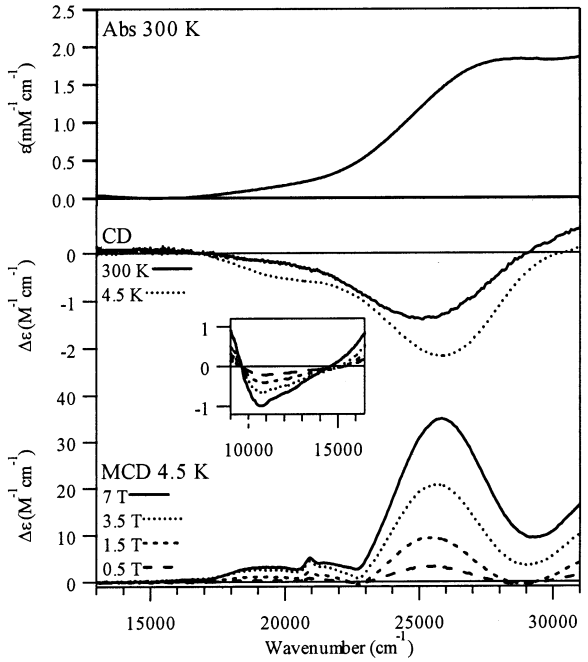

Figure 2. Absorption (top), CD (center), and MCD (bottom) spectra of Fe^{3+}SOD in pH 7 phosphate buffer. Inset: MCD spectra in the near-IR spectral region.

3.2. Fe^{3+}SOD. Spectroscopy. It has previously been observed for Fe^{3+}SOD that increasing pH decreases the intensity of the absorption features in the visible spectral region at ∼370 nm (∼26 000 cm^{-1}).[20] This observed bleaching with a p*K* ∼ 9 has been explained in terms of hydroxide binding to the open coordination site of the resting five-coordinate ferric site.[7] This model is consistent with loss of activity at high pH through competitive inhibition, as the K_m increases at high pH while the k_{cat} is unaffected.[20]

pH 7. Absorption, CD, and MCD spectra obtained for Fe^{3+}-SOD at pH 7 are presented in Figure 2. As Fe^{3+} is a d^5 metal ion, all d → d transitions are formally spin-forbidden and therefore expected to be extremely weak in the absorption spectrum. In contrast, LMCT transitions are typically intense for enzymatic ferric sites (e.g., purple acid phosphatases).[47] Therefore, the absorption band at ∼26 000 cm^{-1} is tentatively assigned as a LMCT transition on the basis of its intensity. This transition is also resolved in the CD and MCD spectra where it gives rise to prominent negative and positive features, respectively.[26] While the absorption spectrum shows no other discern-

(45) Solomon, E. I.; Hanson, M. A. In *Inorganic Electronic Structure and Spectroscopy*; Solomon, E. I., Lever, A. B. P., Eds.; Wiley: New York, 1999; Vol. 2, pp 1−130.
(46) Oganesyan, V. S.; George, S. J.; Cheesman, M. R.; Thomson, A. J. *J. Chem. Phys.* **1999**, *110*, 762−777.
(47) Solomon, E. I.; Brunold, T. C.; Davis, M. I.; Kemsley, J. N.; Lee, S. K.; Lehnert, N.; Neese, F.; Skulan, A. J.; Yang, Y. S.; Zhou, J. *Chem. Rev.* **2000**, *100*, 235−349.

Table 1. Experimental and INDO/S-CI Calculated LMCT Transition Energies,[a] Oscillator Strengths, and ZFS Parameters for Fe^{3+}SOD at pH 7 and 11

	pH 7 Fe^{3+}SOD (experimental)	5-coord Fe^{3+}SOD (predicted)	pH 11 Fe^{3+}SOD (experimental)	6-coord Fe^{3+}SOD (predicted)
d → d[b]	<9000	7600		6600
	10 800	8600		6800
		16 900		8000
		17 400		9900
	19 500 ($f_{exp} = 0.002$)	17 800		12 200
	21 500 ($f_{exp} = 0.003$)	21 000		13 000
		21 300		16 800
		22 600		22 000
Asp → Fe^{3+} LMCT		19 600 ($f = 0.002$)		31 500 ($f = 0.001$)
		20 000 ($f = 0.002$)		31 900 ($f = 0.001$)
	26 000 ($f_{exp} = 0.033$)	20 700 ($f = 0.002$)		32 000 ($f = 0.003$)
		21 100 ($f = 0.063$)	>32 000	34 800 ($f = 0.011$)
		26 600 ($f = 0.025$)		35 400 ($f = 0.086$)
D[c]	−1.7	−3.21	nd[d]	0.24
E/D[c]	0.24	0.17	nd	0.20

[a] LMCT transition energies and ZFS parameters D are given in reciprocal centimeters. [b] Calculated oscillator strengths for d → d transitions are zero, as our computations do not account for spin-orbit coupling among excited states. [c] Experimental ZFS parameters are taken from ref 2. [d] Not determined.

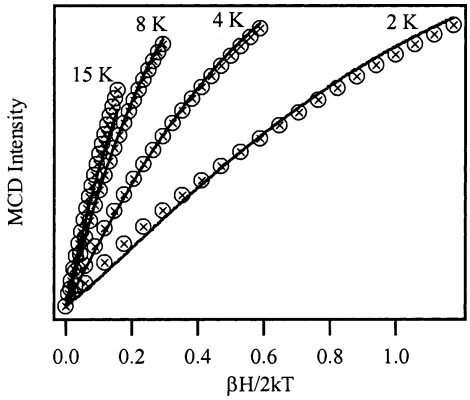

Figure 3. Experimental VTVH MCD data collected at 25 775 cm^{-1} for Fe^{3+}SOD at pH 7 (solid lines) and theoretical fit (⊗). See text for details.

ible features, the CD and MCD spectra reveal additional transitions between 19 000 and 23 000 cm^{-1}. Moreover, in the MCD spectrum, a derivative-shaped feature is observed in the near-IR spectral region centered at ~9500 cm^{-1} (Figure 2, inset). By iteratively fitting both the absorption and MCD spectra (assuming identical Gaussian bandwidth and minor bandshifts), at least three bands were resolved in the 17 000−29 000 cm^{-1} spectral region.[48] Our Gaussian resolution permitted the estimation of experimental oscillator strengths (f_{exp}), where $f_{exp} = 4.32 \times 10^{-9} \int \epsilon(\nu)\, d\nu$, and $\epsilon(\nu)$ is the Gaussian line shape function of the appropriate band. Results from our analysis are presented in Table 1. On the basis of their low absorption intensities, all transitions below 23 000 cm^{-1} are assigned as spin-forbidden d → d transitions that acquire MCD intensity through spin−orbit coupling (vide supra).

While these techniques probe excited states, variable-temperature, variable-field (VTVH) MCD data were collected for Fe^{3+}SOD at pH 7 to gain insight into the ground state of the ferric center. VTVH MCD curves obtained at 25 775 cm^{-1} are shown in Figure 3 (solid lines). These curves are significantly nested; i.e., higher temperature curves saturate more rapidly than lower temperature curves, indicating that the sextet ground state of the ferric ion is subject to large ZFS.

By use of a theoretical model based on the spin-Hamiltonian approach, MCD saturation behavior can be related to g values, ZFS parameters, and transition polarizations.[28,46,49] As EPR experiments have already afforded ZFS values for Fe^{3+}SOD,[2] and for this high-spin ferric system deviations of g from the isotropic free electron value are negligible, we have fit our VTVH data allowing only the transition moment products (i.e., M_{xy}, M_{xz}, and M_{yz}, where x, y, and z refer to the principal axes of the **D**-tensor) to be adjustable parameters. These experimentally determined transition moment products can then be related to the polarization of the electronic transition giving rise to the observed saturation behavior.[28] Fitting of the VTVH data collected at 25 775 cm^{-1} revealed that the relative percentages of x- and z-polarization for this transition are highly correlated. Excellent fits were obtained with 64% x-polarization/36% z-polarization (Figure 3) but also with 2% x-polarization/98% z-polarization (data not shown). Importantly, the addition of any minor component of y-polarization led to significantly poorer fits, indicating that the LMCT transition that is dominant in the absorption, CD, and MCD spectra of Fe^{3+}SOD at pH 7 is polarized perpendicular to the y-axis of the **D**-tensor (see Figure 5 for axis system). This polarization information indicates that this LMCT transition most likely arises from an aspartate → Fe^{3+} CT transition, as the corresponding ligand−metal vector virtually coincides with the x-axis of the **D**-tensor. While this polarization information is also consistent with a hydroxide → Fe^{3+} CT transition or His → Fe^{3+} CT transition involving the axial histidine, the corresponding ligand orbitals are so low in energy that these transitions are expected to occur in the UV region (vide infra).

pH 11. Absorption, CD, and MCD spectra of the high-pH form of Fe^{3+}SOD are presented in Figure 4. Comparing the absorption spectrum of the pH 11 form of Fe^{3+}SOD to that of the pH 7 form reveals significant bleaching of the absorption feature at ~26 000 cm^{-1}, as previously described.[20] While the CD spectra of the high- and neutral-pH forms of Fe^{3+}SOD look qualitatively similar, a comparison of the MCD spectra of the two species gives the most insight into electronic and geometric changes that occur at high pH. While the LMCT band at

(48) As a detailed analysis of all the minor spectral features is not relevant to pK events, we plan to present these results in a forthcoming paper.

(49) Oganesyan, V. S.; Thomson, A. J. *J. Chem. Phys.* **2000**, *113*, 5003−5017.

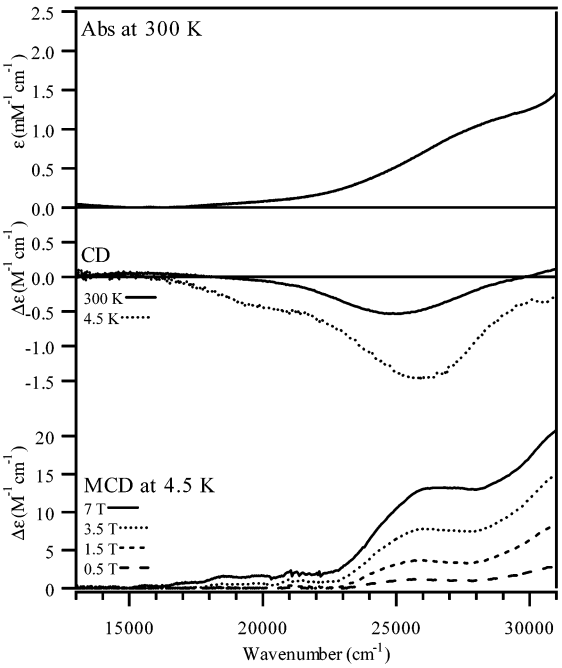

Figure 4. Absorption (top), CD (center), and MCD (bottom) spectra of Fe^{3+}SOD in pH 10 CAPS buffer.

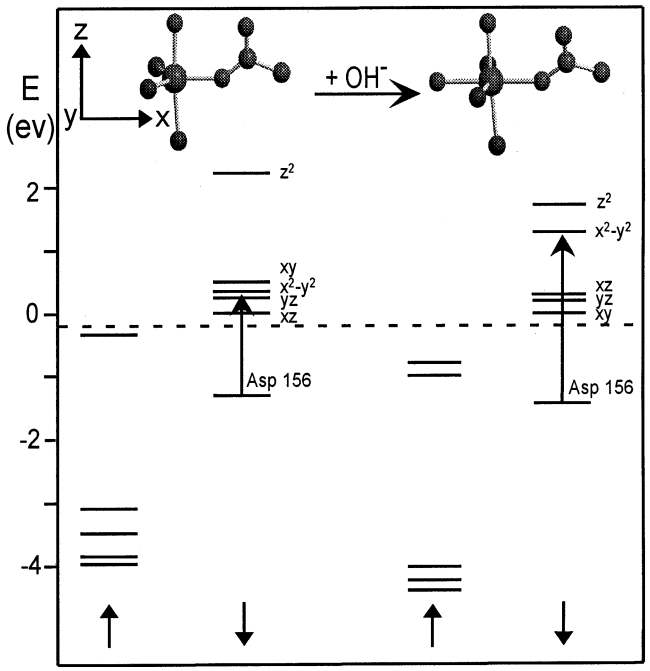

Figure 5. Relevant parts of the MO energy level diagrams obtained from spin-unrestricted DFT calculations on the Fe^{3+}SOD model (left) and the hypothetical six-coordinate Fe^{3+}SOD model possessing an additional hydroxide ligand (right). The models (with hydrogens and second-sphere amino acid residues omitted for clarity) are shown at the top, along with the local coordinate system of the Fe^{3+}SOD model as defined by the principal axes of the INDO/S-CI calculated **D**-tensor. The dominant Asp → Fe CT transition is indicated by an arrow for each case.

$\sim$26 000 cm^{-1} is still present at high pH, it is much less intense and has a slightly different band shape than in the MCD spectrum of the pH 7 species (cf. Figures 2 and 4). Furthermore, an additional, intense positive feature at higher energy (>32 000 cm^{-1}) is evident in the MCD spectrum of the high-pH species (Figure 4). This feature is assigned as another LMCT transition based on its high absorption intensity. The MCD intensity of this feature saturates more rapidly with increasing field than that of the $\sim$26 000 cm^{-1} feature, indicating that two distinct species possessing different ground-state spin Hamiltonian parameters give rise to these features. On the basis of this observation, we propose that the feature at $\sim$26 000 cm^{-1} in the pH 11 spectrum, which saturates in a similar manner to the corresponding band in the MCD spectrum of the pH 7 species (Figure 3), is due to a small fraction of the pH 7 form of Fe^{3+}-SOD (i.e., five-coordinate ferric site). MCD data of the high-pH species collected in the near-IR spectral region showed no contributions from the pH 11 form of the enzyme (data not shown). Overall, these data indicate that the p*K* of $\sim$9 for Fe^{3+}-SOD is associated with a major electronic perturbation of the ferric site as both electronic transition energies and spin Hamiltonian parameters are substantially different below and above this p*K*. To explore the nature of the chemical event associated with this perturbation, DFT and semiempirical INDO/S-CI computations were performed on active-site models of Fe^{3+}SOD at neutral and high pH.

Computations. pH 7. INDO/S-CI computations were performed on an active-site model of Fe^{3+}SOD obtained from the published crystal structure (PDB file 1ISB)[9] and modified as described in the Experimental Section. The relevant output from these computations is summarized in Table 1. All d → d transitions are predicted to have zero intensity, as this method neglects spin−orbit mixing among excited states. However, six LF transitions are predicted between 16 900 and 22 600 cm^{-1}, and two LF transitions are predicted at 7600 and 8600 cm^{-1}, supporting our assignments of the weak MCD bands (Figure 2) as LF transitions. Five low-energy LMCT transitions are predicted, all of which originate from an aspartate-based MO; however, only one of these transitions is predicted to have significant intensity (Table 1).[50] All additional LMCT transition are predicted to occur above 35 000 cm^{-1}. The dominant LMCT transition involves electronic excitation from an MO predominantly (66%) aspartate in character to the Fe $3d_{x^2-y^2}$-derived MO. This transition is predicted to be at 21 100 cm^{-1}, mainly *x*-polarized with a minor *z*-component, which agrees well with experimental polarizations obtained from the fitted VTVH MCD data. In summary, INDO/S-CI computations on the WT active site of Fe^{3+}SOD yield spectroscopic parameters in good agreement with experimental data, illustrating that this method is suitable to evaluate hypothetical active-site models on the basis of spectroscopic data.

We also performed single-point DFT computations on this five-coordinate active-site model of Fe^{3+}SOD. Figure 5 shows a splitting diagram for the Fe 3d-based spin-up and spin-down MOs. As the occupied Fe 3d-based spin-up MOs are significantly stabilized due to spin polarization, they contain significant ligand orbital character. Therefore, the dominant metal−ligand bonding interactions will be inferred from the composition of the unoccupied Fe 3d-based spin-down MOs. As shown in Table 2 and Figure 5, the unoccupied Fe $3d_{z^2}$-derived MO is greatly destabilized relative to the other Fe 3d-based orbitals (as expected for a trigonal bipyramidal species), because it is involved in σ antibonding interactions with the axial hydroxide and histidine ligands. These computational predictions provide

(50) As several LMCT transitions overlap with LF transitions, it is difficult to assign the transitions between 17 000 and 23 000 cm^{-1} in the spectra of Fe^{3+}SOD at pH 7.

Table 2. Relative Energies and Compositions of the Fe 3d-Based Unoccupied Spin-Down Molecular Orbitals Based on a Spin-Unrestricted DFT Calculation on the Fe^{3+}SOD Model

level	relative energy (eV)	Fe 3d (%)	O (hydroxide) (%)	O (Asp)[a] (%)	N(His) (%)
d_{yz}	0	64	10.3	5.5	1.1
d_{xz}	0.2530	74	14	5.5	0.8
$d_{x^2-y^2}$	0.3720	75.6	0.8	10.2	6.7
d_{xy}	0.4601	73.5	7.1	6.3	11.3
d_{z^2}	2.1510	68	13	2.9	19.2

[a] Contributions from both oxygen atoms of the aspartate ligand are considered.

a starting point from which to analyze possible active-site perturbations at high pH.

pH 11. Since previous proposals suggested that binding of a second hydroxide ion is responsible for Fe^{3+}SOD's observed p*K* at ~9,[5,7] a model of the high-pH active site was generated with an equatorial hydroxide ion as a sixth ligand. Because available X-ray crystal structures of hydroxide-bound, six-coordinate ferric sites only exist for cambialistic SODs,[21] a hypothetical model of the active site was generated by using the crystal structure of azide bound to Fe^{3+}SOD from *E. coli* (PDB file 1ISC), replacing the azide with hydroxide, and energy-minimizing the hydrogen-bond network and exogenous ligand positions. INDO/S-CI computations performed on this species predict significantly red-shifted LF transition energies as compared to pH 7 Fe^{3+}SOD. Overall, only two LF transitions are predicted between 16 900 cm^{-1} and 22 600 cm^{-1} for this six-coordinate Fe^{3+}SOD model. This red-shifting of LF transition energies can be understood in terms of the weak-field Tanabe−Sugano diagram for d^5 systems. The five-coordinate ferric site of Fe^{3+}SOD at pH 7 is expected to experience a weaker ligand field (i.e., smaller 10Dq) than the hypothetical six-coordinate site of Fe^{3+}SOD at high pH; thus, the sextet to quartet transitions involving promotion of an electron from e_g to t_{2g} (which formally lowers the one-electron energy by 10Dq) shift to lower energy for the six-coordinate ferric site. Similar to the results obtained for the five-coordinate resting site, INDO/S-CI computations for the six-coordinate ferric site also predict an intense LMCT transition that is still primarily an aspartate (65%) to Fe $3d_{x^2-y^2}$ transition; however, the transition energy is predicted to increase to 35 400 cm^{-1} (Table 1). Thus, the intense feature observed at high energy (~32 000 cm^{-1}) in the high-pH MCD spectrum of Fe^{3+}SOD (Figure 4) is due to the same aspartate-to-iron LMCT transition that gives rise to the dominant feature at ~26 000 cm^{-1} in the low-pH spectrum (Figure 2); its blue shift is the result of binding another hydroxide ligand to the ferric ion at high pH.[7] INDO/S-CI computations on the hypothetical six-coordinate Fe^{3+}SOD active-site model also reveal major changes in ground-state spin Hamiltonian parameters (Table 1), consistent with the strikingly different saturation behavior for the LMCT transition observed in the MCD spectra of the low- and high-pH species. Overall, INDO/S-CI computations on this hypothetical six-coordinate hydroxide adduct are able to account for the key spectral changes observed for Fe^{3+}SOD at high pH.

DFT computations provide further insight into the effects on the splittings and composition of the Fe 3d-derived MOs caused by binding of a sixth ligand to the Fe^{3+}SOD active site (Figure 5 and Table 3). The most notable effects of addition of a sixth ligand to the five-coordinate pH 7 species are the destabilization

Table 3. Relative Energies and Compositions of the Fe 3d-Based Unoccupied Spin-Down Molecular Orbitals Based on a Spin-Unrestricted DFT Calculation on the Six-Coordinate Fe^{3+}SOD Model

level	relative energy (eV)	Fe 3d (%)	O (axial hydroxide) (%)	O (Asp)[a] (%)	N(His) (%)	O (equatorial hydroxide) (%)
d_{xy}	0	82.5	7.2	4.8	0.2	1.4
d_{yz}	0.2759	75.5	17.1	1.7	1.2	1.6
d_{xz}	0.4159	78.2	4.6	3.1	1.2	10.1
$d_{x^2-y^2}$	1.4533	71	0.2	3.4	12.1	9.6
d_{z^2}	1.8248	68.8	14.1	2.8	8.4	2

[a] Contributions from both oxygen atoms of the aspartate ligand are considered.

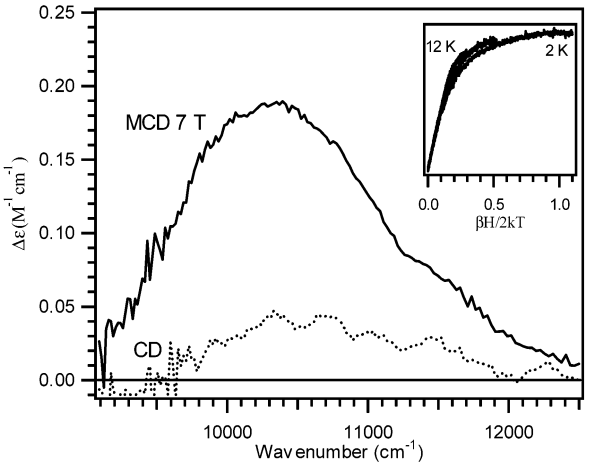

Figure 6. CD and MCD spectra of Fe^{2+}SOD in pH 11 CAPS buffer. Inset: VTVH MCD data obtained at 10 250 cm^{-1} and 2, 4.5, 8, and 12 K.

of the Fe $3d_{x^2-y^2}$- and $3d_{xz}$-derived MOs through σ and π antibonding interactions with the additional hydroxide ion (cf. Table 2). This effect causes the splitting of the Fe 3d-derived MOs to resemble a distorted octahedral pattern (Figure 5), where the Fe $3d_{xy}$, $3d_{xz}$, and $3d_{yz}$ orbitals lie at significantly lower energy than the Fe $3d_{x^2-y^2}$ and $3d_{z^2}$ orbitals. As the dominant LMCT transition involves excitation from an aspartate-derived MO to the Fe $3d_{x^2-y^2}$-based MO, the destabilization of the Fe $3d_{x^2-y^2}$ orbital can account for the blue shift of the LMCT transition (Figure 5).

3.3. Fe^{2+}SOD. Spectroscopy. We have previously shown with NMR spectroscopy that Fe^{2+}SOD undergoes a pH-dependent spectroscopic change with a p*K* of 8.5.[27] It has also been shown that this p*K* is eliminated if tyrosine 34 (Figure 1) is replaced with a phenylalanine by site-directed mutagenesis,[24] supporting the conclusion that deprotonation of tyrosine 34 is responsible for the p*K* of Fe^{2+}SOD.

pH 7. Absorption, CD, and MCD spectroscopic studies on Fe^{2+}SOD at pH 7 by Whittaker and Solomon[51] revealed the presence of one d → d transition at ~10 500 cm^{-1}, consistent with a five-coordinate ferrous site, as was subsequently confirmed crystallographically.[9] Their analysis of VTVH MCD curves permitted estimates of $D = -8 \pm 2$ cm^{-1} and $E/D = 0.27$, consistent with our MCD data obtained on this species.

pH 11. A near-IR MCD spectrum of Fe^{2+}SOD at pH 11 is presented in Figure 6. The dominant feature in this spectrum, centered at ~10 300 cm^{-1}, is assigned as a d → d transition on the basis of its low energy and intensity. The fact that a single

(51) Whittaker, J.; Solomon, E. I. *J. Am. Chem. Soc.* **1988**, *110*, 5329−5339.

Table 4. Experimental and INDO/S-CI Calculated Ligand Field Transition Energies and ZFS Parameters[a] for the Fe^{2+}SOD Active Site at pH 7 and 11

	pH 7 Fe^{2+}SOD (experimental)[b]	5-coordinate Fe^{2+}SOD (predicted)	pH 11 Fe^{2+}SOD (experimental)	Y34 deprotonated Fe^{2+}SOD (predicted)
$d_{yz} \rightarrow d_{xz}$		6400		4700
$d_{yz} \rightarrow d_{xy}$		8400		6900
$d_{yz} \rightarrow d_{x^2-y^2}$		8900		7400
$d_{yz} \rightarrow d_{z^2}$	10 500	12 200	10 300	10 600
D	-8 ± 2	4.7	nd[c]	-5.2
E/D	0.27	0.100	nd	0.124

[a] Ligand field transition energies and ZFS parameters D are given in reciprocal centimeters. [b] Experimental data are taken from ref 51. [c] Not determined.

d → d transition is present in the near-IR region indicates that the active site of Fe^{2+}SOD presumably remains five-coordinate at high pH, as a six-coordinate, distorted octahedral site would be expected to exhibit two d → d transitions centered at ~10 000 cm^{-1}.[52] The MCD intensity of this single transition saturates extremely rapidly, as evident in the VTVH MCD curves (Figure 6, inset). This saturation behavior is similar to VTVH MCD curves collected for Fe^{2+}SOD at pH 7, which also showed rapid saturation and only modest nesting.[51] Overall, spectroscopic data obtained on Fe^{2+}SOD at pH 7 and 11 are strikingly similar, indicating that the pH event with a pK of 8.5 constitutes only a minor perturbation upon the ferrous site.

Computations. pH 7. INDO/S-CI computations performed on an active-site model of Fe^{2+}SOD (PDB file 1ISA)[9] predict four spin-allowed LF transitions from the doubly filled Fe $3d_{yz}$-derived MO to the four singly occupied Fe 3d-based orbitals (Table 4). These computations also predict ZFS values of $D = -4.7$ cm^{-1} and $E/D = 0.100$, in reasonable agreement with experimental data ($D = -8 \pm 2$ cm^{-1} and $E/D = 0.27$).[51]

pH 11. As the Y34F mutant of Fe^{2+}SOD showed no active-site pK,[24] we derived a computational model of the native active site with Tyr34 deprotonated by removing the phenolic proton and using DFT energy minimization to optimize the hydrogen-bond network. To facilitate convergence, a water molecule was added to our hypothetical active-site model, as observed in the X-ray structure, in hydrogen-bond distance to Tyr34.[9,53] ZFS parameters changed little for this model ($D = -5.2$ cm^{-1}, $E/D = 0.124$), while the LF transitions are all predicted to be at slightly lower energy (Table 4). These computational predictions are consistent with our spectroscopy and support our previously developed model[27] that Y34 deprotonation is responsible for the active-site pK of Fe^{2+}SOD.

3.4 Mn^{3+}SOD. Spectroscopy. Though Mn^{3+}SOD has been the subject of much spectroscopic study,[14,54,55] CD and MCD spectroscopies have not previously been used to investigate the chemical nature of the pK events for this enzyme. By optical absorption spectroscopy, two pKs have been observed at 6.9 and 9.7 pH units.[14,56] The pK of 6.9 is associated with minor optical changes and has been tentatively attributed to deprotonation of a histidine side chain. Alternatively, the pK of 9.7 is associated with a decrease in absorption intensity at 21 000 cm^{-1} by 20−30% and a drop in catalytic activity. While the absorption spectrum of the high-pH species resembles the absorption spectrum of the Mn^{3+}SOD fluoride adduct, possibly indicating the coordination of hydroxide ion at high pH, this loss of absorption intensity is noticeably reduced upon site-directed mutagensis of the second-sphere tyrosine 34 residue to phenylalanine,[14] leaving the identity of the high-pH species unclear. As MCD spectroscopy has been shown to be a powerful tool in the study of Mn^{3+}SOD at neutral pH,[57] we have employed it here to explore the nature of the event associated with a pK of 9.7.

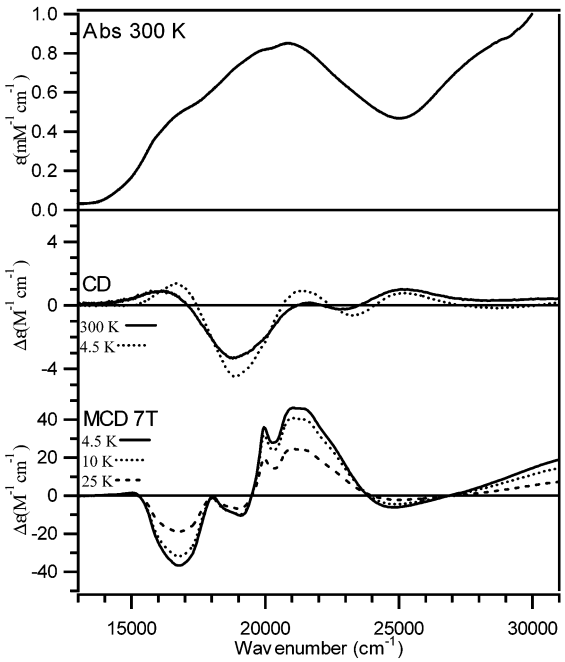

Figure 7. Absorption (top), CD (center), and MCD (bottom) spectra of Mn^{3+}SOD in pH 7 phosphate buffer.

pH 7. Absorption, CD, and MCD spectra of Mn^{3+}SOD are presented in Figure 7. These data are virtually identical to those previously published by Whittaker and Whittaker.[57] Their spectral analysis will be briefly summarized to present a starting point from which to interpret spectral changes at high pH. The broad absorption feature centered at ~21 000 cm^{-1} (Figure 7, top) is composed of four band components, corresponding to the four spin-allowed d → d transitions that involve excitation from one of the four half-filled Mn 3d-derived MOs to the empty Mn $3d_{z^2}$-based MO (Table 5). The CD spectrum also contains four bands, the most intense being located at ~18 900 cm^{-1} (Figure 7, center). On the basis of CD selection rules (vide supra), this feature was assigned as a Mn $3d_{xz} \rightarrow 3d_{z^2}$ transition, as this transition is magnetic dipole-allowed.[57] The MCD spectrum of Mn^{3+}SOD at pH 7 is dominated by a pseudo-A term centered at 20 000 cm^{-1} (Figure 7, bottom), which was attributed to the Mn $3d_{xy} \rightarrow 3d_{z^2}$ and $3d_{x^2-y^2} \rightarrow 3d_{z^2}$ transitions, as the corresponding excited states can mix by spin−orbit coupling to satisfy the MCD selection rule of two perpendicular transition moments.[57] These spectral assignments have been confirmed by single-crystal polarized spectroscopy performed by Whittaker et al.[55] The fine structure observed in the two broad

(52) Solomon, E. I. *Inorg. Chem.* **2001**, *40*, 3656−3669.
(53) Miller, A. F. In *Handbook of Metalloproteins*; Messerschmidt, A., Huber, R., Poulos, T., Wieghardt, K., Eds.; John Wiley & Sons: Chichester, U.K., 2001; pp 668−682.
(54) Whittaker, M. M.; Whittaker, J. W. *Biochemistry* **1996**, *35*, 6762−6770.
(55) Whittaker, M. M.; Ekberg, C. A.; Edwards, R. A.; Baker, E. N.; Jameson, G. B.; Whittaker, J. W. *J. Phys. Chem. B* **1998**, *102*, 4668−4677.
(56) Hsu, J. L.; Hsieh, Y. S.; Tu, C. K.; Oconnor, D.; Nick, H. S.; Silverman, D. N. *J. Biol. Chem.* **1996**, *271*, 17687−17691.
(57) Whittaker, J.; Whittaker, M. *J. Am. Chem. Soc.* **1991**, *113*, 5528−5540.

Table 5. Experimental and INDO/S-CI Calculated d → d Transition Energies and ZFS Parameters[a] for Mn^{3+}SOD, the Hypothetical Six-Coordinate Mn^{3+}SOD Model, and the Y34 Deprotonated Mn^{3+}SOD Model

	Mn^{3+}SOD (experimental)[b]	Mn^{3+}SOD (INDO/S-CI)	HO-Mn^{3+}SOD (INDO/S-CI)	Y34 deprotonated (INDO/S-CI)
d → d	16 720	17 100	8600	16 200
d → d	19 025	19 300	17 500	18 300
d → d	21 040	22 600	22 000	21 500
d → d	23 700	25 200	26 100	23 700
D	2.10	1.94	2.94	1.78
E/*D*	0.114	0.133	0.067	0.168

[a] Transition energies and ZFS parameters *D* are given in reciprocal centimeters. [b] Experimental transition energies are taken from ref 55; ZFS parameters are taken from ref 59.

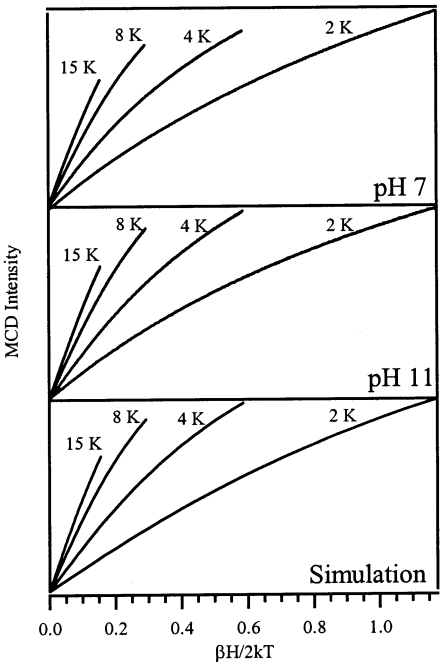

Figure 8. Experimental VTVH MCD data collected at 16 800 cm^{-1} for Mn^{3+}SOD at pH 7 (top) and pH 11 Mn^{3+}SOD (center), and simulated data based on INDO/S-CI computations (bottom).

bands (the positive feature at 18 000 cm^{-1} and the negative feature at 21 000 cm^{-1}) are attributed to spin-forbidden transitions from the quintet ground state to triplet excited states. These spin-flip transitions are expected to be of lower intensity and significantly sharper than the spin-allowed transitions. VTVH MCD curves obtained at 16 800 cm^{-1} show substantial nesting and reveal that the pseudo-*A* term intensity has a nearly linear dependence on field strength (Figure 8, top).

pH 11. Absorption, CD, and MCD spectra of Mn^{3+}SOD at pH 11 are shown in Figure 9. The absorption spectrum of Mn^{3+}-SOD at pH 11 is qualitatively similar to that at pH 7, likewise consisting of a broad peak at ~21 000 cm^{-1} and a shoulder at ~17 000 cm^{-1}. The CD spectrum of Mn^{3+}SOD at pH 11 is also similar to the pH 7 spectrum. Importantly, the two lowest energy transitions observed at pH 7 are clearly conserved in the high-pH CD spectrum. Comparison of the 300 and 4.5 K CD spectra of high-pH Mn^{3+}SOD reveals only minor changes as the temperature is decreased, indicating that the nature of the high-pH species is temperature-independent. This result is significant in light of the fact that the azide adduct of Mn^{3+}-SOD appears to be five-coordinate at physiological temperature,

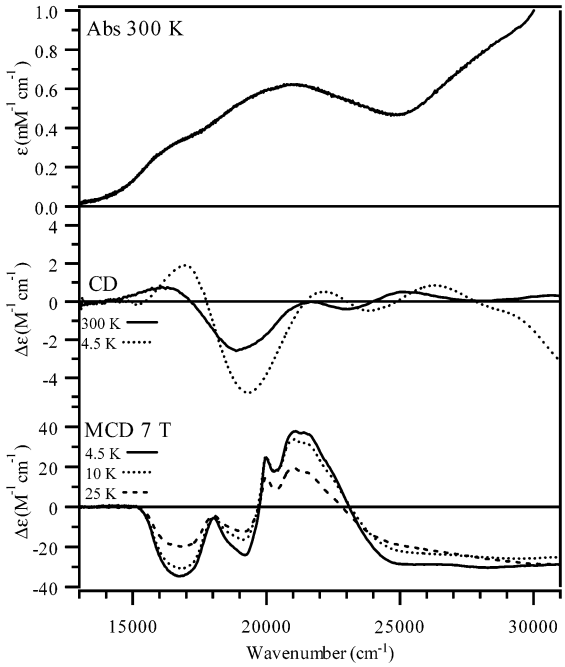

Figure 9. Absorption (top), CD (center), and MCD (bottom) spectra of Mn^{3+}SOD in pH 11 CAPS buffer.

converting to a six-coordinate species at low temperature.[54,58] While our MCD spectra of Mn^{3+}SOD at pH 11 and 7 also appear strikingly similar, some obvious differences are observed above ~24 000 cm^{-1}, where a negative feature is present only in the pH 11 form of the enzyme. This feature is attributed to Mn^{3+} ions that have dissociated from the active site, as MCD data collected on several different high-pH samples exhibited varying intensities for this negative feature. Another slight difference between the two MCD spectra is the higher relative intensity of the negative feature at ~19 000 cm^{-1} in the spectrum of Mn^{3+}SOD at high pH. Despite these minor differences, the pseudo-*A* term that dominates the pH 7 Mn^{3+}-SOD spectrum is still present at high pH. The two species also exhibit virtually identical saturation magnetization curves (Figure 8), illustrating minor ground-state ZFS changes as pH is increased. Overall, absorption, CD, MCD, and VTVH MCD data for Mn^{3+}SOD at pH 7 and 11 are very similar, implying that the manganese active site is only slightly perturbed at high pH.

Azide Adduct. While pH 7 and pH 11 Mn^{3+}SOD are similar spectroscopically, a crystallographically characterized six-coordinate species such as the azide adduct of Mn^{3+}SOD[9] exhibits obvious differences in both ground state and excited-state properties.[57] Variable-temperature MCD spectra of Mn^{3+}-SOD at pH 7 in the presence of excess azide are presented in Figure 10. These spectra are still dominated by a pseudo-*A* term; however, this pseudo-*A* term is shifted in energy, has a strikingly different band shape, and exhibits different intensity saturation behavior (Figure 10, inset) compared to the pseudo-*A* term observed in the MCD spectra of Mn^{3+}SOD at pH 7 and 11 (Figures 7 and 9). These major changes, which reveal conversion to an N_3-Mn^{3+}SOD adduct, have been interpreted in terms of a change in the orbital ground state when azide binds (i.e., empty Mn $3d_{x^2-y^2}$-based MO).[57] Hence, drastic electronic changes

(58) Whittaker, M. M.; Whittaker, J. W. *J. Biol. Inorg. Chem.* **1997**, *2*, 667−671.

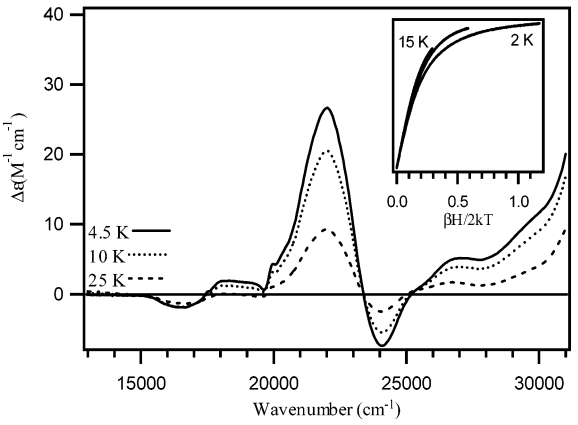

Figure 10. MCD spectrum of N_3-Mn^{3+}SOD adduct. Inset: VTVH MCD data obtained at 22 000 cm^{-1} and 2, 4, 8, and 15 K.

giving rise to major spectroscopic changes are expected when an additional ligand binds to the active-site Mn^{3+} ion.

Computations. pH 7. A model of the Mn^{3+}SOD site was obtained from crystal structure coordinates (PDB file 3MDS), and adjustments in bond lengths were made (Table S5) to account for the redox heterogeneity of this structure.[11] DFT geometry optimizations were carried out to energy-minimize the hydrogen-bond network, and INDO/S-CI computations were performed for this optimized active-site model. The relevant computational output is presented in Table 5. These computations are remarkably accurate in predicting d → d transition energies for the crystallographically characterized neutral-pH form of the enzyme (cf. columns 1 and 2). Additionally, the electronic transitions dominating the MCD spectra are predicted to be predominantly *x*- and *y*-polarized. By use of this polarization as well as published ground-state spin Hamiltonian parameters,[59] the VTVH MCD data can be fit remarkably well (Figure 8, bottom), thus further validating our computational approach.

Whittaker et al.[55] have previously proposed that metal−ligand bonding in Mn^{3+}SOD is dominated by the hydroxide and aspartate 167 ligands. Our DFT results generally support this proposal. The unoccupied Mn 3d-based MO is primarily $3d_{z^2}$ in character and involved in a dominant σ-bonding interaction with the axial hydroxide ligand. As this orbital is the redox-active MO (i.e., the LUMO), its orientation and bonding interactions are crucial to mechanistic proposals.

pH 11. To generate an active-site model of Mn^{3+}SOD with an additional hydroxide ligand, the crystal structure for azide bound to Mn^{3+}SOD (PDB file 1MNG)[9] was used as a starting point, azide was substituted by hydroxide, and the positions of exogenous ligands and the hydrogen-bond network were DFT energy-minimized. The electronic transition energies predicted by INDO/S-CI computations performed on this six-coordinate species differ remarkably from the experimentally determined transition energies (cf. Table 5, columns 1 and 3). Most notably, the first ligand field transition is predicted to shift to lower energy by roughly 8000 cm^{-1}, which implies that such a six-coordinate species would exhibit drastically different spectroscopic signatures than the five-coordinate species present at pH 7.

To validate our calculations on this hypothetical six-coordinate species, computations were also carried out on the crystallographically characterized azide−Mn^{3+}SOD adduct (PDB file 1MNG).[9] As also observed for our hypothetical model of Mn^{3+}SOD at high pH, drastic changes in electronic transition energies are predicted from the INDO/S-CI calculations, the most dramatic of which are the changes in d → d transition energies. In this case, however, our computational results are consistent with our spectroscopic data obtained for N_3-Mn^{3+}-SOD, which show remarkable spectroscopic changes with respect to the five-coordinate Mn^{3+}SOD active site (cf. Figures 7 and 10).

As the high-pH spectra of Mn^{3+}SOD cannot be interpreted satisfactorily in terms of binding of an additional hydroxide ion, we have attempted to rationalize these data in terms of deprotonation of Y34, following a similar approach as presented above for Fe^{2+}SOD. The ligand field transition energies predicted for this species are listed in Table 5. Only subtle changes are expected for this second-sphere perturbation, which seem to correlate well with the minor spectroscopic changes observed at high pH. Furthermore, ligand field transition intensities are predicted to decrease slightly for this species, consistent with the loss of absorption intensity as pH is increased.

3.5 Mn^{2+}SOD. The Mn^{2+} site is similar to the Fe^{3+} site in that both transition metal ions have a d^5 electron configuration. However, no LMCT transitions are observed for the Mn^{2+} ion below 32 000 cm^{-1} as a LMCT transition formally involves a one-electron reduction of the metal ion, which is favorable for Fe^{3+} but not for Mn^{2+}. Additionally, no metal-to-ligand charge transfer (MLCT) transitions are observed[57] as the Mn^{2+}SOD active site contains no low-lying, unoccupied ligand-based orbitals. Therefore, this reduced site is difficult to study with our spectroscopic tools. EPR results indicate that the manganous active site becomes increasingly rhombic as pH is increased (p$K \sim 10.5$).[25] An increase in rhombicity is consistent with the binding of small anions to the metal center, as high-field EPR spectroscopy performed by Un et al.[60] revealed that the axial ZFS parameters decrease upon the binding of azide, while the *E*/*D* ratio increases markedly. Thus, this high-pH event could be associated with hydroxide binding to the active-site metal ion. Alternatively, it could also be ascribed to deprotonation of the coordinated water molecule. To discriminate between these two possibilities, we have generated several hypothetical active-site models from DFT geometry optimizations.

To explore whether the p*K* event of the Mn^{2+}SOD active site may be ascribed to deprotonation of the axial solvent ligand, two hypothetical models of the Mn^{2+}SOD active site, with axial water and hydroxide ligands, respectively, were generated. As it is challenging to predict absolute p*K* values on the basis of computational data, we have used the formalism developed by Noodleman and co-workers[42−44] to estimate the difference in p*K* (Δp*K*) between Mn^{2+}SOD and Fe^{2+}SOD.[61] On the basis of DFT energies of the hypothetical models, we determine a $\Delta pK = -3.6$, indicating that deprotonation of the axial water

(59) Campbell, K. A.; Yikilmaz, E.; Grant, C. V.; Gregor, W.; Miller, A.-F.; Britt, R. D. *J. Am. Chem. Soc.* **1999**, *121*, 4714−4715.

(60) Un, S.; Dorlet, P.; Voyard, G.; Tabares, L. C.; Cortez, N. *J. Am. Chem. Soc.* **2001**, *123*, 10123−10124.

(61) The calculation of absolute p*K* values requires accurately predicted differences in solvation and zero-point energies between deprotonated and protonated states, which is computationally rather difficult. In calculating a Δp*K* we overcome these difficulties by assuming that changes in solvation and zero-point energies are negligible within the SOD family.

molecule is significantly more favorable for Mn^{2+}SOD than for Fe^{2+}SOD. This result can be rationalized in terms of differences in the position of the second-sphere glutamine residue (Figure 1), which is able to hydrogen-bond with coordinated hydroxide but not coordinated water. As the interaction between this Gln residue and coordinated solvent is much stronger (i.e., better oriented for hydrogen bonding) in MnSOD than FeSOD, a coordinated hydroxide molecule is expected to be stabilized through second-sphere amino acids to a much greater extent in MnSOD than in FeSOD.[19] Thus, while the reduced state of the metal ion favors ligation by water, second-sphere amino acids in the MnSOD protein matrix may be able to stabilize ligated hydroxide at high pH.

As no crystal structure is available for any six-coordinate Mn^{2+}SOD adduct, the hypothetical six-coordinate HO−Mn^{2+}-SOD adduct was generated by using the HO−Mn^{3+}SOD active-site model (vide supra) and adjusting the bond lengths for the manganous ion. In this case the ΔpK was calculated relative to Fe^{3+}SOD, as this species most likely binds hydroxide at high pH (vide supra) with a p*K* of ∼8.6. For hydroxide binding to Mn^{2+}SOD relative to Fe^{3+}SOD, we predict a $\Delta pK = 3.96$, indicating that hydroxide binding is less favorable for Mn^{2+}-SOD than Fe^{3+}SOD.

While these computations do not yield a direct, quantitative comparison of deprotonation of the axially ligated water molecule versus hydroxide binding, they do indicate that, for the Mn^{2+}SOD system, second-sphere amino acid residues may allow for deprotonation of the directly coordinated water molecule at high pH.

4. Discussion

Active-site p*K*s for both the reduced and oxidized forms of Fe- and MnSOD were discovered several years ago.[5,14,20,25] However, despite much research in this area, the exact chemical natures of the p*K* events for these enzymes have remained ambiguous. Here we have employed a combination of spectroscopy and computations to study the active sites of reduced and oxidized Fe- and MnSODs at neutral and high pH. Using this combined approach, we conclude that Fe^{2+}SOD and Mn^{3+}-SOD do not bind hydroxide at high pH. For these two species, assignment of the active-site p*K* to Y34 deprotonation results in good agreement between spectroscopic and computational data, whereas computations performed on hypothetical six-coordinate active sites yield spectroscopic parameters that are incompatible with experimental data. In contrast, our hypothetical model of a six-coordinate species for Fe^{3+}SOD yield predicted spectroscopic parameters that agree well with our experimental data collected at high pH. In the case of Mn^{2+}-SOD, our computational data indicate that second-sphere effects cause deprotonation of the coordinated water molecule to be significantly more favorable than for Fe^{2+}SOD; however, our computational results cannot completely rule out the possibility that hydroxide binding may be responsible for this inner-sphere p*K* event.

Our data indicate that knowledge of the oxidation state of the metal ion is crucial when performing studies of active-site p*K*s, as for each SOD there are two distinct p*K* events depending on the oxidation state of the enzyme. Therefore, care must be taken in interpreting crystallographic data of Fe- and MnSOD at high pH, as oxidation state heterogeneity is difficult to avoid in X-ray studies. In view of our results, the partial occupancy (20−43%) for an additional solvent ligand observed in pH 8.5, low-temperature crystal structures of redox heterogeneous crystals of MnSOD[22] could possibly be interpreted in terms of hydroxide binding to the Mn^{2+} site, though even partial occupancy seems unlikely at this pH as p*K* ∼ 10.5 for Mn^{2+}-SOD.[25] Furthermore, our data are inconclusive as to whether the Mn^{2+}SOD active site binds hydroxide at high pH or if the existing, coordinated water molecule is deprotonated. In light of the fact that Børgstahl et al.[22] note that the putative sixth ligand is positioned to hydrogen-bond with Y34 as well as being trapped by a tightly bound additional water molecule that is also involved in hydrogen-bonding with Y34, it seems possible that the putative sixth ligand may actually be a water molecule positioned to hydrogen-bond with deprotonated Y34. Assigning this sixth ligand as a water molecule that only weakly interacts with the metal center would also be consistent with the relatively large oxygen−manganese distance of 2.42 Å.[22] Assignment of this p*K* to Y34 deprotonation could account for the observation that mutation of Y34 to phenylalanine virtually eliminates the Mn^{3+}SOD active-site p*K*.[14] Alternatively, if the active-site p*K* of Mn^{3+}SOD is attributed to hydroxide binding, it would be difficult to rationalize why the Y34F mutation should prevent hydroxide binding. Thus, the additional ligand observed in the active site of MnSOD may not necessarily be indicative of hydroxide binding.

The nature of the active-site p*K*s for both FeSOD and MnSOD seems to indicate that Y34 deprotonation and hydroxide binding to the metal ion are mutually exclusive events. The hydroxide ion still formally has a negative charge even when bound to the active-site metal ion, and its close proximity to Y34 would make deprotonation of the latter electrostatically unfavorable when hydroxide is bound. Alternatively, deprotonation of Y34 creates a negatively charged atom adjacent to the substrate (analogue) binding site. Therefore, binding of a hydroxide ion to the open coordination site of the active-site metal ion is not expected to occur when Y34 is deprotonated.[24] In support of this model, our results indicate that Y34 deprotonation is the active-site p*K* for Mn^{3+}SOD that is associated with a decrease in catalytic activity,[14] possibly indicating that deprotonated Y34 hinders superoxide's access to the active site. For Fe^{3+}SOD (and possibly Mn^{2+}SOD), hydroxide binding occurs at a lower pH than Y34 deprotonation; therefore, hydroxide binding rather than Y34 deprotonation is observed for Fe^{3+}SOD. Alternatively, for Fe^{2+}SOD and Mn^{3+}SOD, hydroxide binding presumably occurs at a higher pH than Y34 deprotonation; therefore, Y34 deprotonation instead of hydroxide binding is observed for these active sites.

Further evidence for this simple model is given by the Fe-substituted form of MnSOD (Fe(Mn)SOD), which is enzymatically inactive. This inactivity has been attributed to a number of factors (vide supra), one of which is competitive inhibition of Fe^{3+}(Mn)SOD by hydroxide at physiological pH [note that the active-site p*K*s of Fe^{3+}SOD and Fe^{3+}(Mn)SOD are ∼9 and ∼6.4, respectively[13b,14,17]]. The p*K* for Fe^{3+}(Mn)SOD has been assigned to hydroxide binding, as the crystal structure of the dimeric protein at pH 8.5 contained one six-coordinate ferric site.[15] Support for this assignment is provided by absorption, CD, and MCD spectra of Fe^{3+}(Mn)SOD obtained at pH 7 and 10 (Figures 11 and 12), which show a similar bleaching at high pH as those of Fe^{3+}SOD (Figures 2 and 4), though the lower

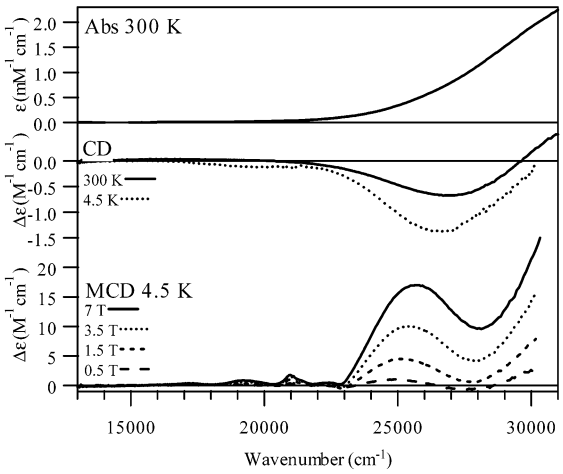

Figure 11. Absorption (top), CD (center), and MCD (bottom) spectra of Fe^{3+}(Mn)SOD in pH 7 phosphate buffer.

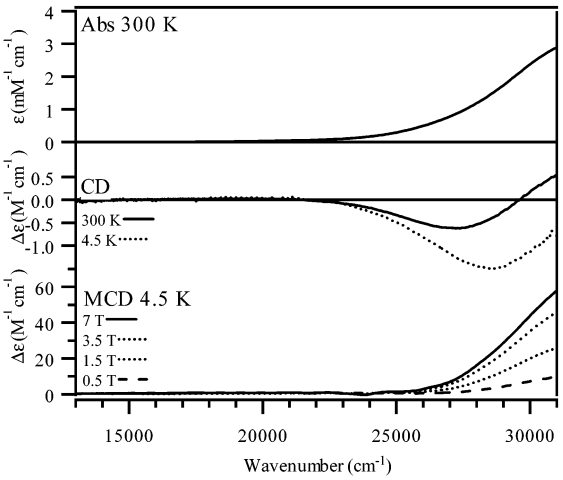

Figure 12. Absorption (top), CD (center), and MCD (bottom) spectra of Fe^{3+}(Mn)SOD in pH 10 CAPS buffer.

p*K* of the metal-substituted enzyme allows for a more complete conversion to the six-coordinate ferric site at pH 10. Therefore, while Y34 is deprotonated in Mn^{3+}SOD at a lower pH than hydroxide binding to the metal ion would occur, the binding of hydroxide to the ferric ion of Fe^{3+}(Mn)SOD occurs at a lower pH than Y34 deprotonation. This result illustrates that hydroxide binding versus Y34 deprotonation is an active-site property that is largely controlled by the identity of the metal cofactor. However, it is intriguing that the p*K* associated with hydroxide binding is lower for Fe^{3+}(Mn)SOD than for Fe^{3+}SOD. The fact that the p*K*s are not identical for both ferric sites indicates that the protein matrix partially tunes the relative stability of a six-coordinate versus a five-coordinate ferric site. This tuning is in part attributed to interactions with tyrosine 34, as the Y34F mutant of Fe^{3+}(Mn)SOD exhibits an active-site p*K* of ~7.9.[14]

The observation that Fe^{3+}(Mn)SOD binds hydroxide at a lower pH than Mn^{3+}SOD seems to imply that the Fe^{3+} ion has, intrinsically, a much higher affinity for hydroxide than the Mn^{3+} ion. This disparity in hydroxide affinity is most likely due to the differences in electronic configuration between the two species. From an inorganic viewpoint, it is not surprising that the $3d^5$ systems (Fe^{3+}- and Mn^{2+}SODs) should act in a different manner with respect to hydroxide ion than the $3d^6/3d^4$ systems (Fe^{2+}- and Mn^{3+}SODs). As hydroxide provides a reasonable

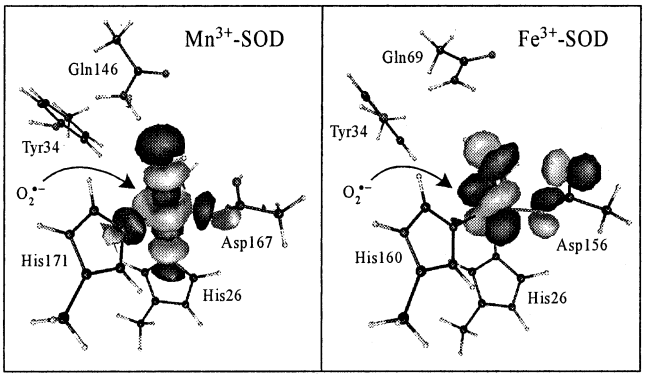

Figure 13. Boundary surface plots of the Mn- (left) and Fe-based (right) MOs that will accept an electron upon reaction with superoxide (eq 1a).

substrate analogue with respect to size and charge, this difference in hydroxide affinity may relate to mechanistic differences between the two enzymes. Previous studies on the substrate analogue azide interacting with the metal active site support this hypothesis.[62] Fe^{3+}SOD forms adducts with azide in which the Fe−N_3 bond angle and the resulting optical spectroscopy can be modified by the FeSOD/N_3 ratio and by site-directed mutagenesis of the second-sphere amino acid residue Q69 (Figure 1). Studies performed on N_3−Mn^{3+}SOD adducts have revealed no such changes as a function of concentration ratios; however, it has been proposed that azide binding results in dissociation of one of the five active-site ligands at room temperature.[57]

On the basis of these differing interactions with substrate analogues and the differences in the nature of p*K* events between Fe- and MnSOD, we hypothesize that the two enzymes may actually use slightly different molecular mechanisms to achieve optimum performance. In the case of trigonal bipyramidal Mn^{3+}SOD, the unfavorable orientation of the Mn $3d_{z^2}$-based redox-active orbital for direct orbital overlap with substrate approaching along the open coordination site between the two equatorial His ligands (Figure 13, left) suggests to us that displacement of the solvent ligand in the putative Mn−superoxo complex might be catalytically important for reorienting the redox-active orbital through a Berry pseudorotation.[54,55,63] In this scenario a square pyramidal complex may be transiently formed in which the Mn $3d_{x^2-y^2}$-based redox-active orbital now has a lobe pointing directly toward the substrate which, along with Asp167 and the two equatorial histidine residues, forms the base of a square pyramid. Thus, a five-coordinate Mn site is maintained which eliminates possible Jahn−Teller contributions to the reorganization energy upon electron transfer. In contrast, the redox active orbital of Fe^{3+}SOD is favorably oriented for a π-bonding interaction with the incoming substrate (Figure 13, right); thus, rapid electron transfer can occur without the need of a major structural rearrangement.

Intriguingly, for both Fe- and MnSODs there appears to be a competition between attracting and repelling small anions at high pH. This competition is ideally balanced in the native Fe- and MnSOD proteins where binding of substrate but not hydroxide occurs at physiological pH. In contrast, Fe^{3+}(Mn)-SOD binds hydroxide to an appreciable extent even at neutral

(62) Xie, J.; Yikilmaz, E.; Miller, A. F.; Brunold, T. *J. Am. Chem. Soc.* **2002**, *124*, 3769−3774.
(63) Berry, R. S. *Rev. Mod. Phys.* **1960**, *32*, 447−454.

pH, which competitively inhibits catalytic activity under physiological conditions. Thus, it appears that the FeSOD and MnSOD protein matrixes impose different properties on their active-site metal ions with respect to small anion interactions. Studies are underway to explore geometric and electronic factors contributing to the different interactions of Fe- and MnSOD with substrate analogues.

Acknowledgment. T.A.J. acknowledges the University of Wisconsin Biophysics Training Grant for financial support. T.C.B. thanks the University of Wisconsin for generous support and acknowledges financial support by NIH (GM G4631) and Dr. Frank Neese (MPI Mülheim) for providing a free copy of ORCA and for useful discussions. A.-F.M. acknowledges financial support by N.S.F. (MCB0129599).

Supporting Information Available: Cartesian coordinates for all computational models and INDO/S-CI active spaces (PDF). This information is available free of charge via the Internet at http://pubs.acs.org.

JA0266058